Photochemical Production of Fe(II) in Rainwater

ARTICLE *in* ENVIRONMENTAL SCIENCE AND TECHNOLOGY · NOVEMBER 2003

Impact Factor: 5.33 · DOI: 10.1021/es030345s · Source: PubMed

4 AUTHORS, INCLUDING:

Rance Hardison
National Oceanic and Atmospheric Administr…
23 PUBLICATIONS **333** CITATIONS
SEE PROFILE

Robert F. Whitehead
University of North Carolina at Wilmington
31 PUBLICATIONS **988** CITATIONS
SEE PROFILE

Joan Willey
University of North Carolina at Wilmington
96 PUBLICATIONS **2,006** CITATIONS
SEE PROFILE

Environ. Sci. Technol. **2003**, *37,* 4610−4616

Photochemical Production of Fe(II) in Rainwater

R. J. KIEBER,* D. R. HARDISON, R. F. WHITEHEAD, AND J. D. WILLEY

Department of Chemistry, University of North Carolina at Wilmington, Wilmington, North Carolina 28403-3297

Significant concentrations of Fe(II) were produced upon irradiation of authentic rainwater with simulated sunlight. The magnitude of photoproduction was dependent on initial Fe(II), Fe(III), and hydrogen ion concentrations, with more Fe(II) photoproduction when initial Fe(III) and H^+ concentrations were high and initial Fe(II) concentrations were low. An equation was developed that accurately predicts photoproduction of Fe(II) in rainwater based on initial Fe speciation values and pH. The quantum yield of Fe(II) photochemical production in rain decreased dramatically with increasing wavelength and decreasing energy of incoming radiation with the average quantum yield at 265 nm approximately an order of magnitude greater than at 546 nm. Probable photochemical precursors of Fe(II) in authentic rain include iron(III) oxalate, iron(III) hydroxide, and an undefined Fe(III) complex. The wavelength-dependent Fe(II) production was modeled using the average Fe(II) efficiency spectrum, an average rainwater absorption spectrum, and the modeled actinic flux for temperate latitudes in both summer and winter. The response spectrum has the highest photoproduction of Fe(II) in summer and winter at 325 and 330 nm, respectively, with greater production in summer rain due to increased actinic flux and longer hours of irradiation.

Introduction

Iron is one of the most abundant trace elements in atmospheric waters. It has been measured in fog, snow, cloudwater, and rain (*1, 2*). Iron is involved in many important redox reactions that occur in the troposphere such as the generation of hydrogen peroxide in cloudwater (*3, 4*) and fog (*3, 5*) and the interconversion of S(IV) to S(VI) in the troposphere (*6*−*8*). Iron also contributes to the oxidizing capacity of the troposphere by its reactivity with several free radicals including $^{\bullet}OH$, $^{\bullet}HO_2$, and $^{\bullet}O_2^-$ (*4, 9*−*11*). Iron is also involved in the reactions of several organic pollutant compounds in the troposphere (*10, 12, 13*) and in the redox chemistry of several trace metals (*10, 12, 13*).

Despite the significance of Fe speciation in atmospheric waters, the mechanisms controlling that speciation are unclear. Earlier studies have suggested that photochemical processes may be important in controlling Fe speciation in atmospheric waters. Many atmospheric redox reactions involving Fe, including those with hydrogen peroxide, organic compounds, and trace metals are thought to be photochemically driven (*2, 14*−*17*).

The seasonal and diurnal variability of the Fe(II) to Fe(III) ratio in rainwater at geographically diverse locations suggests that photochemistry affects Fe speciation in rain (*2, 14, 16*). The ratio of Fe(II)(aq)/Fe(III)(aq) was highest in Wilmington, NC, rain received between noon and 6 p.m. with much less Fe(II) during late evening and early morning hours (*2*). Diurnal and seasonal variations in rainwater iron speciation were also observed during a summer and winter cruise aboard the R/V *Endeavor* at the Bermuda Atlantic Time Series Station (*16*). There was a 200-fold higher Fe(II)(aq)/Fe(III)(aq) ratio in rain received between noon and 6 p.m. relative to late evening or early morning rain in summer rain at BATS (*16*). In New Zealand rain, which experiences higher UV irradiation than North Carolina or BATS, all dissolved iron was Fe(II) with no Fe(III) detected (*2*).

The precise photochemical processes responsible for the seasonal, diurnal, and geographical variability of Fe in rainwater are not well-defined at this time. Earlier research has focused on photochemical conversions of Fe(III) complexes with organic acids with high concentrations of reactants to simulate cloudwater (*3*). The focus of this study is to explore photochemistry as a potentially important process controlling the speciation of iron in rainwater under environmentally relevant concentrations of iron and other potentially important reactants.

Materials and Methods

Reagents and Standards. All bottles and containers used for standards and samples were thoroughly cleaned before use employing previously described trace metal clean protocols (*18*−*20*). Poretics polycarbonate filters used for filtration (0.4 and 0.1 μm) were first rinsed with DI water, placed in 6 M Optima HCl for at least 1 week, and thoroughly rinsed with DI water prior to use.

All reagents were Fisher Scientific reagent grade (Fairlawn, NJ) except ferrozine (3-(2-pyridyl)-5,6-bis(4-phenylsulfonic acid)-1,2,4-triazine), which was SigmaUltra (>99.9% pure) grade. All water for standards and reagents was obtained from a Milli-Q/Milli-Q Ultra Plus (MQ) (>18 MΩ·cm^{-1}) water system (Millipore, Bedford, MA). Synthetic rain for standard preparation (pH 4.5) was prepared daily by diluting 4 mL of 5 mM trace metal grade H_2SO_4 to 1 L with MQ water.

Rain filtration, preparation of all standards and samples for iron analysis, and reagent storage were prepared and processed in a class 100 laminar flow clean bench to minimize contamination. An acidified secondary stock solution of 36 μM Fe was prepared gravimetrically each month from a dilution of a 18 mM iron standard obtained from Fisher Scientific and stored in the dark at 4 °C. Total iron standards were prepared gravimetrically daily from the 36 μM secondary stock solution and diluted with pH 4.5 synthetic rain. An acidified Fe(II)(aq) primary stock solution (10 mM) was prepared by dissolving 0.4970 g of ferrous chloride in 250.0 g of MQ water followed by storage at 4 °C for up to 2 weeks. A Fe(II)(aq) secondary stock solution (10 μM) was prepared gravimetrically daily by diluting the primary stock solution. Working standards were prepared daily by dilutions of each secondary stock.

Sample Collection and Storage. Rain filtration, standard and sample preparation, and reagent storage were all conducted in a class 100 laminar flow clean bench. Rainwater samples were collected on an event basis using three Aerochem Metrics (ACM) model 301 automatic sensing wet/dry precipitation collectors equipped with high-density polyethylene (HDPE) buckets. The collector used for Fe samples had a trace metal clean HDPE funnel placed in the wet deposition bucket. Tygon tubing with a fluoropolymer FEP (inert) liner connected the funnel to a trace metal clean

* Corresponding author telephone: (910)962-3865; fax: (910)962-3013; e-mail: Kieberr@uncw.edu.

10.1021/es030345s CCC: $25.00
Published on Web 08/15/2003

2-L Teflon bottle inside a closed HDPE bucket. After each event the Teflon bottle was replaced with a freshly washed bottle, and the funnel and tubing were thoroughly rinsed with MQ water. The Teflon bottle containing the rain event was returned to the lab within 5 min of collection. Blanks performed with MQ water in place of rainwater had undetectable Fe concentrations. The remaining two collectors housed 4-L muffled glass beakers in the sample buckets and were used for collection of supporting data.

Analytical Methods. Fe(II) and Fe(III) were determined by a modification of the ferrozine method (*21*). The 30-mL aliquots of rainwater were filtered through a precleaned 0.4-μm polycarbonate filter. Filtered blanks performed with MQ water in place of rainwater had undetectable Fe concentrations. To determine total dissolved Fe concentrations, 700 μL of hydroxylamine hydrochloride (1.4 M) was added to a filtered sample and set aside for at least 1 h to ensure complete reduction of Fe(III)(aq) to Fe(II)(aq). Ferrozine (700 μL, 10 mM), a reagent that reacts with Fe(II)(aq) forming a colored complex, was added and thoroughly mixed with the sample followed by addition of 1.8 mL of pH 5.5 ammonium acetate buffer to adjust pH. Fe(II)(aq) concentrations were determined by the same procedure except hydroxylamine hydrochloride was not added to the filtered samples. Addition of ferrozine reagent to Fe(III) standards resulted in no measurable Fe(II) signal after 1-h storage, indicating that the reagent did not reduce any Fe(III) to Fe(II) within the time frame of these analyses.

Absorbance of the iron ferrozine complex was read at 562 nm using a 1-m (Ocean Optics) or 5-m (World Precision Instruments) liquid waveguide capillary cell (LWCC) attached to an Ocean Optics SD2000 spectrophotometer and an Analytical Instrument Systems model DT 1000 CE UV/vis light source. Fiber optic cables carried light from the source to the cell and from the cell to the spectrometer. Absorbance measurements were also made at 700 nm and subtracted from analytical results to correct for absorbance due to turbidity or baseline drift (*22*). Fe(III)(aq) was calculated from the difference between total dissolved Fe and Fe(II)(aq). A conservative detection limit based on three times the signal-to-noise ratio for both Fe(II) and Fe(III) is 0.4 nM.

Supporting Data. Rainwater pH was determined using a Ross model 81-02 electrode. Orion low ionic strength buffers (6.97/4.10) were used to calibrate the instrument, and 50 μL of pHisa ionic strength adjuster was added to each 5 mL of sample to match the ionic strength of samples to that of buffers. Dissolved organic carbon (DOC) was determined using a Shimadzu 5000 TOC analyzer with an ASI 5000 autosampler (*23*). The detection limit for DOC in rainwater is 7 μM based on three times the standard deviation of the blank. Hydrogen peroxide analyses were done using a scopoletin-induced fluorescence decay technique (*24*, *25*).

Experimental Procedures

Photolysis experiments were performed using a Spectral Energy Corp. solar simulator (LH 153 lamp housing, 1-kW Xe arc lamp, LPS 256 SM power supply) equipped with an AM1 filter to remove unwanted wavelengths. The spectral quality and intensity of the solar simulator is very similar to that of midsummer, noontime solar irradiance for 34° N latitude. Filtered rainwater samples were apportioned into 2 cm i.d. × 10 cm path length cylindrical quartz cells with Teflon stoppers. Aliquots were collected for initial Fe concentrations just before the start of each irradiation. Identical samples were placed in the dark and served as controls. A constant flow−temperature bath surrounded light-exposed cells in order to maintain constant temperature during irradiation. Photochemical experiments were run at the temperature of the rain at the time of collection. Dark controls were kept at the same temperature as irradiated samples. Light measurements at individual cell locations were made with an Ocean Optics SD2000 spectrophotometer connected to a fiber optic cable terminated with a CC−UV cosine collector. The system was calibrated with a NIST traceable tungsten lamp, and data were collected with OOIrrad software.

Quantum yields of Fe(II) production in rainwater were determined using a Spectral Energy Corp. monochromatic irradiation system (LH 151 lamp housing, 1-kW Hg−Xe arc lamp, LPS 256 SM power supply, GM 252−20 high-intensity 0.25 m grating monochromator). The photolysis experiments involved isolating specific wavelengths and irradiating samples for predetermined time periods. Slit widths of 1.5 mm were used at the entrance and exit, which produced a band-pass of 5 nm. Wavelengths corresponding to peak output from the Hg−Xe lamp (265.2, 300, 313, 365, 404.5, 435, and 546 nm) were chosen to minimize irradiation times. All wavelengths above 400 nm had a 400 nm long pass filter in place to minimize effects of second-order light. Irradiation time (1−60 min) was determined experimentally to ensure an easily measured increase in Fe(II) was observed but kept short enough to avoid depletion of Fe(III) and photobleaching of the sample. All samples were measured for initial concentrations of Fe(II) just before the start of each experiment. Immediately following irradiation, final Fe(II) concentrations were determined in irradiated and dark control samples. Samples were irradiated in 10-cm quartz cells, and light was detected using an International Light IL1700 radiometer (5 V bias off) with a SED033 detector. Light measurements were calibrated for the system using a conventional potassium ferrioxalate actinometer (*26*).

The Fe(II) quantum yield data were modeled in order to estimate quantum yields at wavelengths other than those actually measured. Following previous studies of environmental photochemistry (*27*), we assume an exponential shape for the model and employ the following formula for interpolation:

$$\phi_\lambda = \exp^{-(m_1 + m_2[\lambda - 300])} \quad (1)$$

where ϕ is quantum yield, m_1 and m_2 are fitting parameters from a nonlinear least-squares regression performed with SystStat 10.2, and λ is wavelength in nanometers. The model is based on work by Cullen and Neale (*28*) and Rundel (*29*) and has been shown to be very robust for use in environmental photochemistry (*30*, *31*). The TUV model developed by Madronich was used to estimate actinic flux as a function of latitude, time, and atmospheric conditions in modeling calculations (*32*).

Results and Discussion

Photoproduction of Fe(II). Photochemical experiments were conducted to determine the influence of sunlight on the speciation of iron in rainwater. Twelve authentic rainwater samples were irradiated for 2 h under the solar simulator, and the speciation of iron was measured and compared to dark controls (Table 1). The initial iron speciation values as well as dissolved organic carbon concentration (DOC), pH, and hydrogen peroxide were all measured immediately prior to irradiation. The date of collection and time interval of the rain event are also given in Table 1. These temporal data give information about the photochemical history of samples that may effect initial iron speciation values observed just prior to irradiation (*1*, *2*). Samples were irradiated either immediately after collection or after storage at 4 °C for less than 1 week.

Photoproduction of Fe(II) after 2 h in light-exposed flasks was observed in 10 of 12 rain samples as compared to dark controls. There was an increase of Fe(II) in several dark controls possibly because of dark thermal reduction of Fe(III)

TABLE 1. Fe(II) Concentration (nM) in Rainwater Initially and after 2-h Irradiation or 2-h Dark Storage[a]

date	time interval	Fe(II) initial (nM)	Fe(III) initial (nM)	Fe(II) light (nM)	Fe(II) dark (nM)	ΔFe(II) (nM)	DOC (μM)	pH	H_2O_2 (μM)	ΔH_2O_2 (μM)
12/10/00	1830−0800	46.0	17.0	50.4	52.2	−1.8	31	4.50	21.2	0.6
3/13/01	2100−0700	18.3	4.1	19.1	16.3	2.8	39	4.74	23.0	−1.0
3/21/01	0600−0800*	1.9	3.4	2.7	1.1	1.6	7	5.47	12.0	na
3/29/01	0500−1330	13.0	8.5	21.5	18.5	3.0	26	4.35	25.1	na
4/25/01	0500−1600	13.7	15.0	23.7	15.0	8.7	16	4.62	15.8	−0.7
6/15/01	1200−0600**	13.0	8.5	21.5	18.5	3.0	26	4.67	26.6	3.1
8/14/01	0000−1030	5.9	22.5	21.2	4.8	16.4	30	4.29	10.5	na
8/19/01	1800−2230	61.8	10.0	60.3	60.3	0.0	34	3.73	20.1	−0.9
8/30/01	1500−0500	30.0	260	167	23.4	144	39	4.46	9.9	−1.4
8/31/01	1600−2000	23.7	18.3	41.3	30.4	10.9	54	4.07	19.1	2.4
9/4/01	1300−1600	5.9	6.4	4.8	2.7	2.1	14	5.47	10.9	na
9/6/01	2000−0100	5.4	7.0	7.8	4.7	3.1	40	4.80	20.4	3.0

[a] ΔFe(II) is the difference between Fe(II) concentrations in light-exposed rain vs dark controls. The corresponding values for Fe(III) (nM), DOC (μM), pH, and H_2O_2 (μM) at the beginning of the irradiation are also given along with the change in concentration of H_2O_2 over the course of the irradiation. The date of collection and time interval of the rain event are presented. * indicates a rain event over 26 h, and ** indicates rain from tropical Storm Alison, which occurred over 42 h. All other storms were shorter than 24 h. na, final analysis not performed, so the change could not be calculated.

species by superoxide radicals, hydrogen peroxide, or organic compounds (*33*). The role of superoxide in iron speciation in rainwater, however, cannot be easily delineated as many other species effectively compete with iron for the reactive radicals, especially Cu (*3*) ,which occurs in concentrations on the same order of magnitude as iron in rainwater. The rate of dark thermal reduction of Fe(III) is much slower than corresponding photochemical production rates (*33*), which is consistent with the results presented in Table 1. The photochemical production of Fe(II) reported in Table 1 may explain why the ratio of Fe(II)(aq)/Fe(III)(aq) was highest in rainwater received between noon and 6 p.m. in earlier iron speciation studies because this is the period of greatest sunlight intensity (*2, 16*).

Irradiation of rain samples resulted in photochemical reduction of up to 73% of the dissolved Fe(III), with much variation between samples (Table 1). These are net reduction rates as some reoxidation of Fe(II) probably occurred during the 2-h irradiation via oxidation by hydrogen peroxide, $HO_2^{\bullet}$, or superoxide radicals. The rate of reoxidation, however, is difficult to assess in these samples because oxidation kinetics with synthetic iron solutions do not accurately predict the rate of oxidation of Fe(II) in authentic rain samples. Oxidation of Fe(II) in solutions of inorganic Fe(II) salts by H_2O_2, $^{\bullet}O_2^-$, or $HO_2^{\bullet}$ occurs in minutes (*33*). However, the concentration of Fe(II) in authentic rain is stable for more than 24 h, so it is not comparable to simple inorganic Fe(II) with respect to oxidation kinetics (*1, 16*).

The pH in irradiated rain events remained constant before and after photolysis in all samples; therefore, production of Fe(II) was not dependent on pH changes caused by irradiation. The concentration of hydrogen peroxide in the rainwater samples prior to irradiation was between 10 and 27 μM. There were variable changes in hydrogen peroxide concentrations in light-exposed flasks; however, these changes were generally quite small (less than 10%) and were inconsistent with production in some events and decay in others. Therefore, it is unlikely that changes in peroxide concentrations caused by irradiation had any significant impact on photoproduction of Fe(II).

Analysis of the data in Table 1 by sequential linear regression indicates that the magnitude of Fe(II) photoproduction was dependent on initial Fe(II), Fe(III), and hydrogen ion concentrations, with more Fe(II) photoproduction when initial Fe(III) and H^+ concentrations were high and initial Fe(II) concentrations were low. The concentrations of other potentially important rainwater parameters, including DOC and hydrogen peroxide, did not affect

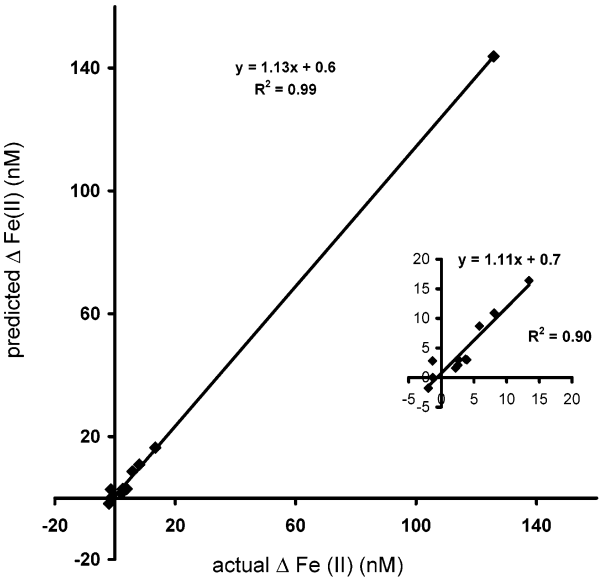

FIGURE 1. Comparison of actual Fe(II) photoproduction in rainwater vs that predicted (nM) using eq 2: $n = 12$, $r^2 = 0.998$, and $p < 0.001$. The inset represents the same correlation with the highest data point at 135 nM iron removed.

the extent to which Fe(II) was photoproduced in these samples.

A equation that accurately predicts photoproduction of Fe(II) in rainwater from initial Fe speciation values and pH was developed using forward stepwise linear regression followed by multiple linear regression:

$$\Delta[\mathrm{Fe(II)}]_{\mathrm{nM}} = 0.798 + 0.570[\mathrm{Fe(III)}]_{\mathrm{nM}} - 0.287[\mathrm{Fe(II)}]_{\mathrm{nM}} + 0.0565[\mathrm{H^+}]_{\mu\mathrm{M}} \quad (2)$$

where $n = 12$, $p < 0.001$, and $r^2 = 0.998$ (Figure 1). The insert in Figure 1 represents the same data set with the high value at approximately 135 nM removed. The strong positive correlation is almost identical regardless if this point is included or removed, indicating that this correlation does not depend only on this one high data point. The change in [Fe(II)] did not correlate significantly ($r^2 < 0.5$) with [Fe(III)], [Fe(II)], or [H^+] when considered one at a time; therefore, no single variable can predict Δ[Fe(II)]. This strong dependence of iron photoproduction on initial Fe(II), initial Fe(III), and H^+ is important because it may allow prediction of Fe(II)

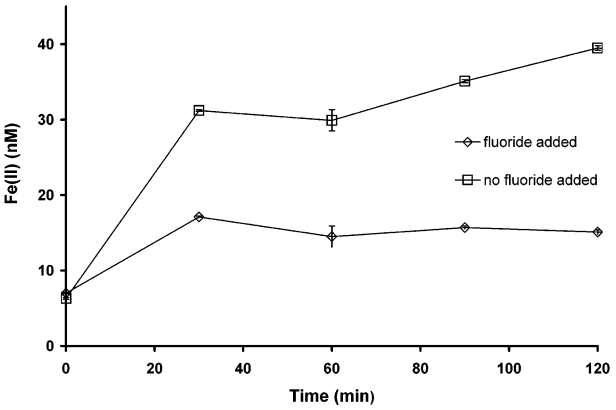

FIGURE 2. Concentration of Fe(II) (nM) as a function of irradiation time in authentic rainwater (pH 4.60) with and without added fluoride (1 mM). Initial conditions in the authentic rainwater were as follows: DOC = 135 μM, Fe(II) = 20 nM, Fe(III) = 84 nM, and H_2O_2 = 10 μM. Error bars represent ± 1 SD based on n = 3.

photoproduction capacity in rain samples from other geographical regions if the initial iron speciation and pH values are known. This equation should not be applied to other matrixes such as cloudwater, freshwater, or seawater with significantly different pH, peroxide, and DOC concentrations or under different irradiation conditions where its validity has not been tested.

Photolysis Experiments with Addition of Fluoride. Photolysis experiments were conducted on authentic rain samples to determine the mechanism of Fe(II) photoproduction. Fluoride (1 mM final concentration) was added to authentic samples (typically containing $<1\,\mu$M F^-) because it forms a complex with Fe(III) that has no ligand-to-metal charge transfer in aqueous solution. The net result is that the Fe−fluoride complex is not photochemically reactive because fluoride is a poor electron-donating ligand (*34*). There was more photoproduction of Fe(II) from authentic rain without fluoride than with fluoride after 2-h irradiation; however, there was some photoproduction in both solutions (Figure 2).

Equilibrium speciation calculations (MINEQL+, equilibrium constants were the same as in ref *35*) were performed for this rain sample, which had pH 4.60, 55 nM Fe(III), 7 nM Fe(II), and in this experiment 1 mM F^-. Calculations were adjusted for ionic strength, which came primarily from the added NaF. These calculations indicate that Fe(III) would occur in combination with fluoride, primarily as FeF_3^0(aq) (18 nM) and FeF_2^+(aq) (14 nM) and with 22 nM occurring as $Fe(OH)_2^+$(aq). Inclusion of 0.1 μM humic acid type Fe(III) binding sites as done in ref *2* ($pK_a = 5$ and $\log K_{FeHum} = 12$) in the rain matrix used for the MINEQL+ calculation leaves 14 nM as FeF_3^0(aq) plus 11 nM as FeF_2^+(aq), with 11 nM as iron humate and 18 nM $Fe(OH)_2^+$(aq). Therefore, not all the Fe(III) was complexed with fluoride under these conditions leaving approximately half in a photochemically active form, which allowed photochemical production of 9 nM Fe(II) in the sample to which fluoride was added as compared with 34 nM in the rain with no added fluoride. The difference in the concentration of Fe(II) photoproduced in the rain with and without fluoride was very close to the concentration of photoreactive Fe(III) remaining in the rain after addition of fluoride regardless of whether humics are included in the rain matrix. This suggests that the mechanism of Fe(II) production in rainwater involves a primary photoprocess where an iron complex absorbs light directly and produces Fe(II) as a product.

Another important conclusion that can be drawn from Figure 2 is that in irradiation of authentic rain (i.e., no added fluoride) the rate of Fe(II) photoproduction decreased markedly with time. The majority of the ferrous iron was produced in the first 30 min, after which many fewer moles of Fe(II) were produced with time. The photoproduction of Fe(II) appears to follow pseudo-first-order kinetics in this optically thin authentic rain sample. This is consistent with eq 2, which predicts that as Fe(III) is depleted by production of Fe(II), the magnitude of ferrous iron production would decrease accordingly. Over time, as concentrations of Fe(II) precursors become depleted and Fe(II) concentration build up, the rate of production of Fe(II) decreases.

TABLE 2. Characteristics of the Four Rain Events Used in the Quantum Yield Determination of Fe(II) Production in Rainwater[a]

event no.	Fe(II) initial (nM)	Fe(III) initial (nM)	pH	H_2O_2 (μM)	Abs_{300}	DOC (μM)
329	7.2	17.0	4.82	16.0	0.0443	na
330	21.2	38.6	4.40	5.1	0.0463	110
331	58.2	77.2	4.36	na	0.0730	95
332	6.7	36.3	5.98	0.6	0.0545	19

[a] Abs_{300} is the baseline-corrected absorbance of the rain event at 300 nm in a 10-cm cell. na indicates not analyzed.

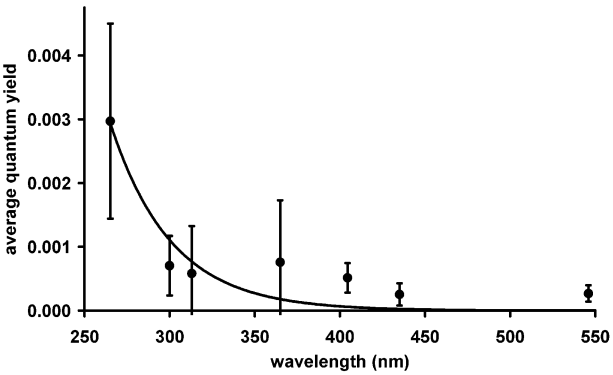

FIGURE 3. Average quantum yield from four different rain events plotted as a function of irradiation wavelength. Error bars represent ± 1 SD based on n = 4. The curve is a plot of eq 1 as discussed in the text.

Quantum Yield Determinations. Four different rain events were photolyzed with monochromatic irradiation in order to measure the efficiency or quantum yield of Fe(II) photoproduction. The relevant rainwater characteristics of each sample are presented in Table 2. Quantum yield, defined as moles of Fe(II) produced per mole of photons absorbed, is a unitless value for measuring the efficiency of specific wavelengths at initiating a photochemical response. The current study differs from many other photochemical studies in that the exact compound responsible for the photochemical reaction is not known, and it is almost certain that other moieties in the samples are also absorbing light in processes unrelated to iron chemistry. Therefore, previous studies have used the term "apparent" quantum yield for data from experiments using natural water samples (*31*).

An efficiency spectrum, defined as apparent quantum yield as a function of wavelength, was produced to determine the spectral dependence of Fe(II) photoproduction. The efficiency spectrum was generated by plotting the average apparent quantum yield from four separate rain events as a function of wavelength (Figure 3) and employing eq 1 to generate a model ($r^2 = 0.929$) with fitting parameters of 6.9 and 0.034 for m_1 and m_2, respectively. The quantum yield decreased dramatically with increasing wavelength and decreasing energy of incoming radiation. The average quantum yield at 265 nm was approximately an order of

magnitude greater than at 546 nm, although there was still production even at these longer wavelengths.

The solar simulator experiments demonstrated that Fe(II) production slowed with increases in irradiation time. Quantum yield irradiation times were purposely kept to a minimum to avoid depletion of Fe(III) reactants. Some of the variability in apparent quantum yield data may thus result from exposure history of samples and its resulting speciation characteristics when it was collected. Nevertheless, the efficiency spectrum developed in this study in conjunction with measured absorbance and light data can be used to reliably predict Fe(II) production over short time periods. For example, in the first 30 min of exposure for the authentic sample without F^- (Figure 2), an increase of 25 nM Fe(II) was observed. Multiplying the absorbed dose (over 30 min) for this sample by the model efficiency spectrum and integrating over wavelength yields a predicted production of 28 nM Fe(II). Obviously, this model should not be applied to experiments with longer irradiations because production becomes a nonlinear function of time (Figure 2).

Mechanism of Fe (II) Photoproduction. Earlier studies with primarily synthetic solutions suggest that several photoprocesses could be responsible for production of Fe(II) in authentic rainwater samples. Photodegradation of iron(III) hydroxide complexes in synthetic solutions, for example, will rapidly produce Fe(II) (*33*). Production of significant quantities of Fe(II) from iron hydroxide complexes in the authentic rain samples studied here, however, is unlikely to be the dominant source of Fe(II). Iron hydroxide complexes at environmentally relevant rainwater concentrations and pH values have very weak absorbances past 400 nm. Using published molar extinction values (*36*) and quantum yields (*33*), photodegradation of iron(III) hydroxides produces essentially no Fe(II) beyond 313 nm. Photodegradation of ferric hydroxide species therefore may account for some of the Fe(II) produced in rainwater at the very short wavelengths, but it is most likely not the dominant source as significant production of Fe(II) was observed in authentic rain samples even past 500 nm.

Photolysis of iron(III) oxalate complexes are another potentially significant source of Fe(II) in rainwater. Iron(III) oxalate species are predicted to complex as much as 95% of the Fe(III) in rainwater under environmentally relevant concentrations of reactants, primarily as $Fe(C_2O_4)_2^-$, with small amounts of $Fe(C_2O_4)^+$ and $Fe(C_2O_4)_3^{3-}$ (*2*). Wavelength-dependent Fe(II) production rates in authentic rain samples were therefore compared to predicted production rates assuming that photodegradation of iron(III) oxalate primarily $Fe(C_2O_4)_2^-$ was the primary source of Fe(II) (Table 3). The predicted Fe(II) in Table 3 was calculated for the four rain events used in the quantum efficiency (Figure 3) assuming that 10%, 25%, 50%, and 100% of the Fe(III) in rain was complexed with oxalate. Predicted Fe(II) rates were calculated from known quantum yield (*26*) and molar extinction values for iron(III) oxalate (*36*). The exact iron(III) oxalate species present is not important because they have similar absorption spectra and quantum yields (*36*, *37*). Regardless of the complexation capacity of oxalate chosen, the quantity of Fe(II) produced via oxalate photodecomposition does not agree with the Fe(II) photoproduced in authentic rain samples over the wavelength range investigated. At low wavelengths, significantly more Fe(II) would be produced by photodecomposition of iron(III) oxalate than was observed while at longer wavelengths not enough Fe(II) would be produced. This suggests that, while photodecomposition of iron(III) oxalate species may contribute to production of Fe(II) in authentic rainwater, they are not the only source. This assessment is similar to the conclusion drawn regarding HOOH production via photodecomposition of iron(III) oxalate compounds in atmospheric waters. In synthetic solutions HOOH is efficiently produced upon irradiation of iron(III) oxalate compounds (*36*). Comparison of wavelength-dependent quantum yields in authentic cloudwater assuming that iron oxalate was the primary source of HOOH with those of those of synthetic solutions in a manner similar to presented in Table 3, however, indicated that iron oxalate was not the primary source of HOOH in the authentic sample (*37*).

TABLE 3. Wavelength-Dependent Fe(II) Production Rates (nM/Irradiation Period) Measured in Authentic Rain Samples and Calculated Assuming Photodegradation of Iron(III) Oxalate Was the Primary Source of Fe(II)[a]

wavelength	measured E329	10% FeOx	25% FeOx	50% FeOx	100% FeOx
300	6.2	14	35	70	141
313	7.0	35	87	173	347
365	6.8	19	48	96	193
404	2.6	1	4	7	14
435	3.8	0	0	1	1
546	3.5	0	0	0	0
wavelength	**measured E330**	**10% FeOx**	**25% FeOx**	**50% FeOx**	**100% FeOx**
313	23.9	736	1821	3641	7282
404	15.8	34	85	170	340
546	1.3	0	0	0	1
wavelength	**measured E331**	**10% FeOx**	**25% FeOx**	**50% FeOx**	**100% FeOx**
300	70.0	271	677	1355	2717
313	56.5	261	654	1307	2621
365	61.4	75	188	376	754
404	43.3	47	118	236	474
435	39.7	5	12	23	47
546	14.6	0	0	1	2
wavelength	**measured E332**	**10% FeOx**	**25% FeOx**	**50% FeOx**	**100% FeOx**
300	8.2	102	254	508	1017
313	7.7	84	209	418	836
365	9.4	140	349	698	1396
404	6.1	31	78	156	312
435	4.8	2	5	10	20
546	2.0	0	0	0	1

[a] The percentages indicate the extent of complexation of Fe(III) by oxalate used in the calculation of production rates presented in this table. Event (E) numbers are the same as in the previous table.

The results presented in Table 3 suggest that another Fe(III) ligand is responsible for much of the photochemical production of Fe(II) observed in authentic rain samples. One potentially significant class of Fe(III) ligands in rainwater is humic-like substances. Model calculations indicate that complexation of iron with humic-like compounds is extensive in rainwater (ca. 50%) over the typical rainwater pH range from 4.0 to 5.0 (*2*). The complexation of Fe(III) by humics in rainwater could be significant because they are very efficient chromophores and rapidly photodegrade under ambient sunlight conditions (*38*).

To assess the importance of humic substances in the photoproduction of Fe(II), an authentic rain sample and a synthetic rain sample with and without addition of 1 mg L^{-1} Cape Fear River humics (isolated via C18 extraction; *39*) were irradiated for 2 h under the solar simulator (Figure 4). The humic substances used in the experiments were extracted from the Cape Fear River, which is within 10 km of our rainwater collection site. How representative they are of rainwater ligands is unknown; however, they are from the same geographical region and have undergone similar climate conditions. Initial conditions in the authentic rainwater were as follows: at pH 4.5, DOC = 135 μM, Fe(II) = 10 nM, Fe(III)

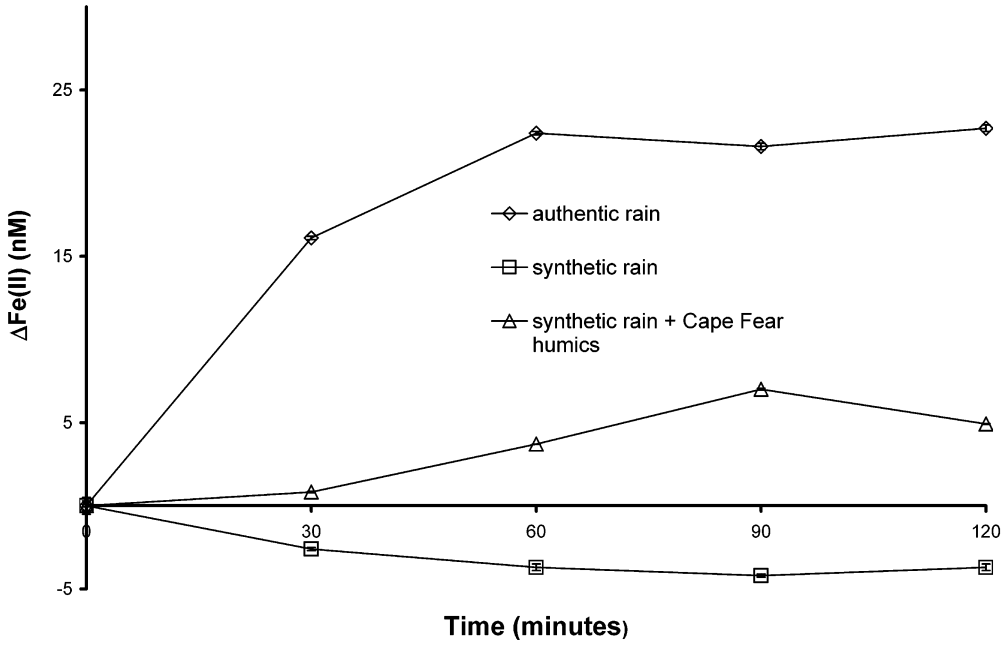

FIGURE 4. Change in concentration of Fe(II) (nM) as a function of irradiation time in authentic rainwater and in synthetic rainwater with and without added humics (1 mg L^{-1}). Initial conditions in the authentic rainwater were as follows: at pH 4.5, DOC = 135 μM, Fe(II) = 10 nM, Fe(III) = 38 nM, and H_2O_2 = 10 μM; in synthetic rain at pH 4.5, DOC = 12 μM when humics were present and approximately 2 μM when humics were not added, Fe(II) = 8 nM, Fe(III) = 12 nM, and H_2O_2 = 10 μM. Error bars represent ± 1 SD based on n = 4.

= 38 nM, and H_2O_2 = 10 μM, and in the synthetic rain at pH 4.5, DOC = 12 μM when humics were present and approximately 2 μM when humics were not added, Fe(II) = 8 nM, Fe(III) = 12 nM, and H_2O_2 = 10 μM. Fe was added to both synthetic rain matrixes as chloride salts. No iron spike was added to the authentic rain sample.

There was a significant increase in Fe(II) upon 2-h irradiation of authentic rain similar to what was observed earlier (Table 1). The concentration of Fe(II) in synthetic rain without added humics decreased with time as the Fe(II) was slowly oxidized over the 2-h incubation, again indicating no significant photoproduction by iron(III) hydroxides, the only potential chromophore present in this solution. The concentration of Fe(II) in the synthetic rain with 1 mg L^{-1} added humics more than doubled upon irradiation. Addition of humic substances to synthetic rain, therefore, caused the synthetic rain to mimic the authentic rain upon irradiation. This indicates that at least some of the photoproduction of Fe(II) in authentic rainwater may involve humic-like ligands via a primary photoprocess.

Modeling Studies. The modeled efficiency spectrum was multiplied by the absorbed dose rate (wavelength-dependent local, 34° N at 7.5 km altitude, actinic flux multiplied by an average rainwater absorbance spectrum) to develop a wavelength-dependent response spectrum of photoproduced Fe(II) during winter and summer (Figure 5). The response function is given in units of nM h^{-1} of noontime sun and was calculated in optically thin solutions as $2.303\mathrm{Abs}_\lambda I_\lambda \phi_\lambda$ where Abs_λ is the absorbance in cm^{-1}, I_λ is the actinic flux in mol of photons cm^{-2} h^{-1}, and ϕ_λ is the quantum yield at a given wavelength. The response spectrum has the highest photoproduction of Fe(II) for summer and winter at 325 and 330 nm, respectively. In winter, the small change in solar spectral distribution resulting from increased atmospheric absorption due to longer path lengths (lower sun angle) slightly shifts Fe(II) photoproduction to longer wavelengths. As indicated by the seasonal differences, the pattern of greater quantum efficiency and higher rainwater absorbance with decreasing wavelength suggests that Fe(II) photoproduction will be sensitive to atmospheric conditions, such as ozone levels, which change the solar spectral distribution.

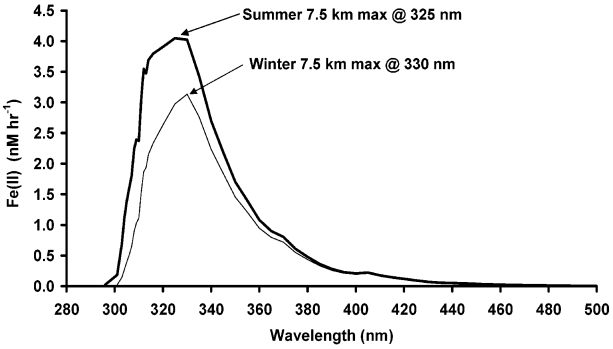

FIGURE 5. Response spectra of Fe(II) photoproduction per hour of noontime sun in rain drops at an altitude of 7.5 km during both summer and winter.

In addition to a wavelength dependency of the response spectrum of photoproduced Fe(II), there is also a distinct seasonality to the photochemical production. Rainwater drops in summer photoproduce significantly more Fe(II) relative to winter months. This seasonal dependence to the response spectrum is due primarily to the greater intensity of the actinic flux, especially at UV wavelengths, and would be accentuated by longer hours of irradiation during summer months, possibly up to the point where Fe(III) precursors are completely exhausted, as was observed in New Zealand rain (*2*).

Acknowledgments

This work was supported by NSF Grant ATM-9729425 and ATM-0096878. The Marine and Atmospheric Chemistry Research Laboratory group at UNC Wilmington assisted with sampling and analyses.

Literature Cited

(1) Kieber, R. J.; Williams, K. H.; Willey, J. D.; Skrabal, S. A.; Avery, G. B. *Mar. Chem.* **2001**, *73*, 83−95.
(2) Willey, J. D.; Kieber, R. J.; Williams, K. H.; Crozier, J. S.; Skrabal, S. A.; Avery, G. B. *J. Atmos. Chem.* **2000**, 185−205.
(3) Zuo, Y.; Hoigne, J. *Environ. Sci. Technol.* **1992**, *26*, 1014−1022.

(4) Sedlack, D. L.; Hoigne, J. *Atmos. Environ.* **1993**, *27A*, 2173−2185.
(5) Zuo, Y.; Deng, D. *Geochim. Cosmochim. Acta* **1999**, *63*, 3451−3455.
(6) Graedel, T. E.; Weschler, C. J.; Mandich, M. L. *Nature* **1985**, *317*, 240−242.
(7) Jacob, D. J.; Waldman, J. M.; Munger, J. W.; Hoffmann, M. R. *J. Geophys. Res.* **1986**, *91*, 1089−1096.
(8) Breytenbach, L. W.; Vanpareen, W.; Pienaar, J. J.; van Eldik, R. *Atmos. Environ.* **1994**, *28*, 2451−2459.
(9) Faust, B.; Hoigne, J. *Atmos. Environ.* **1990**, *24A*, 79−89.
(10) Faust, B.; Zepp, R. G. *Environ. Sci. Technol.* **1993**, *27*, 2517−2522.
(11) Siefert, R. L.; Hoffmann, M. R. *J. Geophys. Res.* **1996**, *101*, 14441−14449.
(12) Erel, Y.; Pehkonen, S. O.; Hoffmann, H. *J. Geophys. Res.* **1993**, *98*, 18423−18434.
(13) Zuo, Y. *Geochim. Cosmochim. Acta* **1995**, *59*, 3123−3130.
(14) Kieber, R. J.; Peake, B.; Willey, J. D.; Jacobs, B. *Atmos. Environ.* **2001**, *35*, 6041−6048.
(15) Kieber, R. J.; Rhines, M. F.; Willey, J. D.; Avery, G. B. *Atmos. Environ.* **1999**, *33*, 3659−3667.
(16) Kieber, R. J.; Willey, J. D.; Avery, G. B. *J. Geophys. Res.* (in press).
(17) Kieber, R. J.; Willey, J. D.; Zvalaren, S. D. *Environ. Sci. Technol.* **2002**, *36*, 5321−5327.
(18) Bruland, K. W.; Franks, R. P.; Knauer, G. A.; Martin, J. H. *Anal. Chim. Acta* **1979**, *105*, 223−245.
(19) Bruland, K. W. *Earth Planet. Sci. Lett.* **1980**, *47*, 176−198.
(20) Tramontano, J. M.; Scudlark, J. R.; Church, T. M. *Environ. Sci. Technol.* **1987**, *21*, 749−753.
(21) Stookey, L. C. *Anal. Chem.* **1970**, *42*, 779−781.
(22) Waterbury, R. D.; Wensheng, Y.; Byrne, R. H. *Anal. Chim. Acta* **1997**, *357*, 99−102.
(23) Willey, J. D.; Kieber, R. J.; Eyman, M. S.; Avery, G. B. *Global Biogeochem. Cycles* **2000**, *14*, 139−148.
(24) Kieber, R. J.; Helz, R. G. *Anal. Chem.* **1986**, *58*, 2312−2315.
(25) Kieber, R. J.; Cooper, W. J.; Willey, J. D.; Avery, G. B. *J. Atmos. Chem.* **2001**, *39*, 1−13.
(26) Murov, S. L.; Carmichael, I. H.; Hug, G. *Chemical Actinometry*; Marcel Dekker: New York, 1993.
(27) Whitehead, R. F.; de Mora, S. *Marine Photochemistry and UV Radiation*; The Royal Society of Chemistry: Cambridge, 2000; Vol. 14.
(28) Cullen, J. J.; Neale, P. J. *Biological Weighting Functions for Describing the Effects of Ultraviolet Radiation on Aquatic Systems*; R. G. Landes Co.: Georgetown, TX, 1997.
(29) Rundel, R. D. *Physiol. Plant* **1983**, *58*, 360−366.
(30) Johannessen, S. C.; Miller, W. L. *Mar. Chem.* **2001**, *76*, 271−283.
(31) Miller, W. L.; Moran, M. A.; Sheldeon, W. M.; Zepp, R. G.; Opsahl, S. *Limnol. Oceanogr.* **2002**, *47*, 343−352.
(32) Madronich, S.; Flocke, S. *The Role of Solar Radiation in Atmospheric Chemistry*; Springer-Verlag: Heidelberg, 1998; Vol. 2, Part L.
(33) Faust, B. In *Aquatic and Surface Photochemistry*; Helz, G. R., Zepp, R. G., Crosby, D. G., Eds.; Lewis Publishers/CRC Press: Boca Raton, FL, 1994; pp 3−39.
(34) Gao, H.; Zepp, R. G. *Environ. Sci. Technol.* **1998**, *32*, 2940−2946.
(35) Stumm, W.; Morgan, J. J. *Aquatic Chemistry: Chemical Equilibria and Rates in Natural Waters*; Wiley and Sons: New York, 1996.
(36) Zuo, Y.; Hoigne, J. *Environ. Sci. Technol.* **1992**, *26*, 6.
(37) Arakaki, T.; Anastasio, C.; Shu, P. G.; Faust, B. *Atmos. Environ.* **1995**, *29*, 1697−1703.
(38) Kieber, R. J.; Zhou, X. Z.; Mopper, K. *Limnol. Oceanogr.* **1990**, *35*, 1503−1515.
(39) Kieber, R. J.; Li, A.; Seaton, P. J. *Environ. Sci. Technol.* **1999**, *33*, 993−998.

Received for review February 3, 2003. Revised manuscript received June 30, 2003. Accepted July 9, 2003.

ES030345S